

A Comparison of Model and Observed Turbulent Kinetic Energy within Coastal Barrier Jets Forced by Landfalling Cyclones

Joseph B. Olson* and John M. Brown
NOAA Earth System Research Laboratory, Boulder, CO, US

1. Introduction

The coastal region of western North America frequently experiences intense orographically enhanced wind and rainfall when cyclones make landfall. Strong barrier jets can form when onshore flow becomes blocked and deflected by the coastal mountains (Macklin et al. 1990; Overland and Bond 1993 and 1995; Loescher et al. 2006; Olson et al. 2007). Coastal jets have been shown to nearly double in width when inland cold pools are accelerated through the coastal mountain gaps and merge with the ambient barrier jet to produce a hybrid barrier jet (Olson et al. 2007; Olson and Colle 2008). Turbulence associated with coastal jets can produce wind gusts sufficiently strong to cause damage to residential and commercial property.

There have been few studies on the turbulence within barrier jets. Karacostas and Marwitz (1980) documented the observed turbulent kinetic energy (TKE) over Elk Mountain, Wyoming for partially blocked flow ($Fr \sim 1$). The TKE upwind of the barrier had a maximum at the surface and was generated by a combination of shear and buoyancy production below mid-mountain-level. Bond and Walter (2002) documented the TKE in a low-level jet within weakly blocked flow ($Fr \sim 3$) off the coast of Oregon; this TKE was produced mainly by shear. They noted countergradient momentum fluxes, which may have been caused by non-local mixing of a highly patchy distribution of TKE within the vicinity of the jet.

To our knowledge, there have been no detailed studies of the TKE within a barrier jet produced by strongly blocked flow or that may have been influenced by gap outflows from coastal mountain gaps. Also, few companion modeling studies have been attempted to help diagnose the mechanisms responsible for redistributing the momentum within the barrier jet. The ability of current and next-generation operational weather forecast models to simulate the inland cold pools, their subsequent formation of coastal gap outflows, and their interaction with coastal barrier jets needs to be

assessed.

The National Center for Environmental Prediction (NCEP) currently employs the Rapid Update Cycle (RUC; Benjamin et al. 2004), which uses 1-h assimilation at 13-km grid spacing to provide mesoscale guidance for short-range forecasts. Among the many significant weather phenomena, the RUC is relied upon for the prediction of turbulence and high speed wind events by the marine and aviation industries. The current RUC modeling system will be replaced with a new high-frequency system, the Rapid Refresh (RR; Benjamin et al. 2006), with operational transition at NCEP planned for 2009 or 2010. The RR forecast model component will be the Advanced Research version of the Weather Research and Forecasting Model (WRF-ARW; Skamarock et al. 2005). The current RUC domain will be expanded in the RR to cover a larger North American domain, which will include the complex orography of Alaska and Canada. Also, new planetary boundary layer (PBL) schemes are being developed and compared to current operational schemes. Model errors over this expanded region are relatively unknown, especially for short-range forecasts as produced by the RUC or RR, and need to be identified and diagnosed in order to further system development.

This study investigates the performance of the WRF-ARW over the complex coastal orography of Alaska, with focus on the spatial and temporal structure of the TKE and the fluxes of heat and momentum within coastal barrier jets. High-resolution model simulations are compared with TKE and flux measurements within a barrier jet sampled by the Wyoming King-air research aircraft during the Southeastern Alaskan Regional Jets (SARJET) field experiment. Some questions this study attempts to address are the following:

- How well can the WRF-ARW simulate the coastal barrier jets and the associated TKE along the coastal orography of Alaska?
- How is the TKE distributed relative to the jet for both classical and hybrid barrier jets?
- How do the simulated TKE structures change with resolution?
- What limitation does the relatively coarse 13-km grid spacing planned for the WRF-RR place on performance in the vicinity of steep coastal terrain?

* Corresponding author address: Dr. Joseph B. Olson,
NRC Research Associate, NOAA Earth System Research
Laboratory, Mail Code R/GSD-1, 325 Broadway, Boulder,
CO, 80305. Email: joseph.b.olson@noaa.gov

2. Methodology

a. Model Configuration

The WRF-ARW was configured for three domains: 13, 4.33, and 1.44 km, using one-way nesting (Fig. 1). Each domain consisted of 51 full sigma levels in the vertical, such that the coarse domain has equivalent vertical and horizontal resolution to the current RUC and RR. The coarse domain is large enough to capture the landfalling cyclones and moderately resolve a typical barrier jet with width $O(100\text{ km})$. Also, the coarse domain provides a benchmark for testing the expected advantage of the high-resolution nests, which better resolve the complex coastal orography and mountain-induced circulations.

The initial and boundary conditions were provided by NCEP Global Forecast System (GFS) analyses at 0.5-deg resolution every 6 hours. The sea-surface temperatures were obtained from the daily NCEP SST analysis. The Mellor-Yamada-Janjic (MYJ; Janjic 2002) PBL scheme was applied along with a Monin-Obukhov-based surface layer scheme and the RUC land-surface model. The Grell-Devenyi cumulus parameterization (Grell and Devenyi 2002) was used on the 13-km domain, while the precipitation was explicitly resolved in the nests using the Thompson six-class microphysical scheme (Thompson et al. 2004 with enhancements). The Rapid Radiative Transfer Model (RRTM; Mlawer et al. 1997) was used to parameterize radiative processes. This model also employs a gravity wave absorption layer in order to prevent gravity waves from being reflected off the model top.

b. Data processing

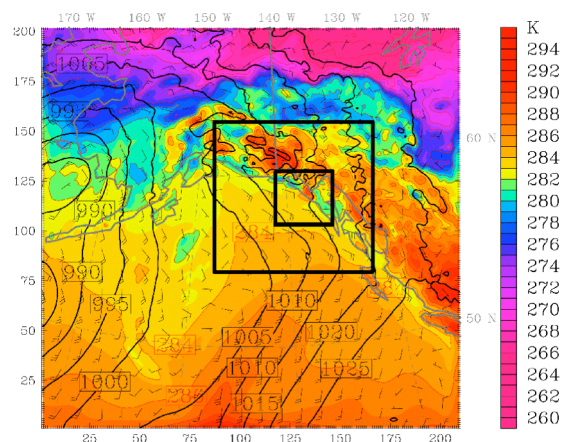


Figure 1. The 13-, 4.33-, and 1.44-km domains with SLP (black contours), potential temperature (color) and wind barbs valid at 1800 UTC 12 October 2004.

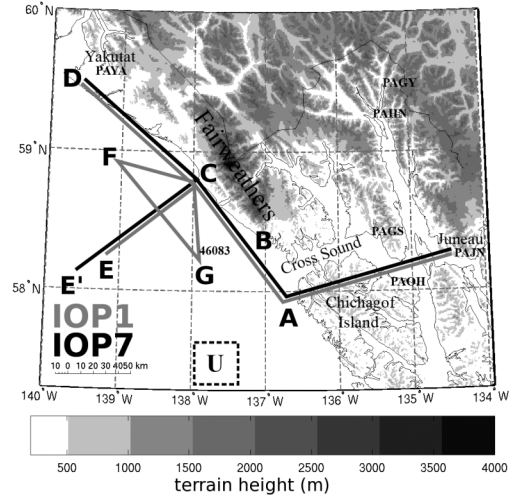


Fig. 2. SARJET study region showing the flight tracks (IOP 1 gray and IOP 7 black) and terrain (gray shaded). The dashed box around U is used to estimate model flow parameter upstream of the Fairweathers

Flight-level measurements for SARJET were obtained from the University of Wyoming's King-Air research aircraft. These measurements consisted of in situ observations from south of Cross Sound (pt. A in Fig. 2) to near Yakutat (pt. D), and from four southwest-northeast flight legs at various altitudes near the coast (pt. C) to 75 – 120 km offshore (E or E'). This flight pattern was completed twice (in two separate flights) for each IOP, and will be referred to as flight 1 and flight 2, respectively.

Flight data sampled at 10-Hz was used to compute fluxes of momentum in the mean along-wind $[\rho(u'w')]$ and crosswind $[\rho(v'w')]$ directions, sensible $[C_p\rho(T'w')]$ and latent heat $[L\rho(q'w')]$ fluxes, and TKE $[(u'^2 + v'^2 + w'^2)/2]$. Here u' , v' , and w' are the along-wind, crosswind, and vertical wind perturbations, respectively; ρ is air density; and C_p and L are the specific heat and latent heat of vaporization, respectively. Both the fluxes and TKE were calculated using the covariance method. The mean thermodynamic and kinematic properties, TKE, and turbulent fluxes were obtained from 30 s averages along the flight legs transecting the barrier jet. This averaging period yields independent estimates separated by roughly 3 km in the horizontal direction and an average of 150 m in the vertical direction. This extended abstract will focus on the hybrid barrier jet of SARJET IOP7.

3. Results

a. Overview of IOP7

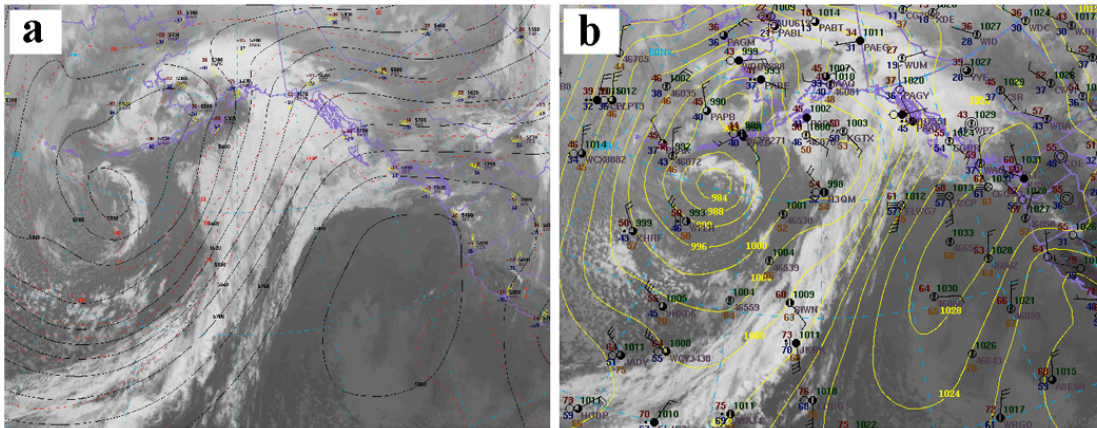


Figure 3. IR satellite image at (a) 1200 UTC 12 Oct 2004 with GFS 500 mb geopotential height (black every 60 meters) and observations from upper-air stations and (b) 1800 UTC 12 Oct 2004 with GFS sea level pressure analysis (yellow every 4 mb) and surface observations.

At 1200 UTC 12 October 2004 (Fig. 3a), there was a deep upper-level low over the Aleutian Islands with ridging over the Alaskan-Canadian Coast. At 1800 UTC (Fig. 3b), a surface cyclone (982 mb) was near the southern tip of the Alaskan Peninsula, while a secondary low (~998 mb) over the central Gulf of Alaska was moving eastward towards the SARJET study area. A 1028 mb surface high over western Canada resulted in an off-shore pressure gradient, which accelerated cold continental air through the coastal mountain gaps. The corresponding model solution for this time (Fig. 1) accurately captures the depth and placement of the large-scale features.

By 0000 UTC 13 October 2004 (not shown), the secondary low pressure came within 500 km of the coast and had intensified to 995 mb. The combination on onshore ambient flow with the addition of the cold gap outflow resulted in a strong coastal jet near 30 m s^{-1} .

b. Wyoming King-Air flight measurements

The observed winds were near coast-parallel during the first flight of IOP7 (Fig. 4a). As the cold air flowed over slightly warmer sea-surface temperature (SST), weak surface heat fluxes resulted in buoyancy-generated TKE beneath 250 m ASL. This combined with shear-generated TKE in the surface layer to produce TKE of $0.5\text{-}2.0 \text{ m}^2 \text{ s}^{-2}$ in the lowest flight leg (Fig. 4a).

During flight 2, the cyclone and associated offshore trough moved into the coastal region, shifting the ambient winds more southerly (Fig. 4b). A strong shear layer developed between the maximum gap outflow (~300 m MSL) and the weaker southerly flow aloft (~1000 m MSL). This resulted in a reduction of the local Richardson

number to ~ 0.25 . The observed maximum TKE increased to $2\text{-}5 \text{ m}^2 \text{ s}^{-2}$ and became elevated to the top of the gap outflow (400-500 m ASL). The TKE observed in the lowest flight leg ($\sim 200 \text{ m ASL}$) remained significant and was still dominated by buoyancy production.

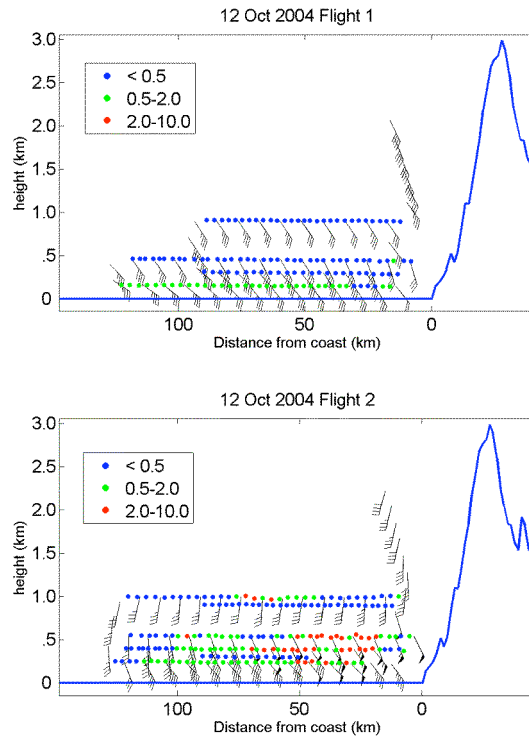


Figure 4. Flight measurements of winds (full barb = 10 kts or $\sim 5 \text{ m s}^{-1}$) and TKE (colored dots) along multiple flight legs between points C and E (Fig. 1). Upper panel shows the measurements taken during the first flight (1800-2100 UTC) and the lower panel shows the second flight (2300-0230 UTC) on 12-13 October 2004.

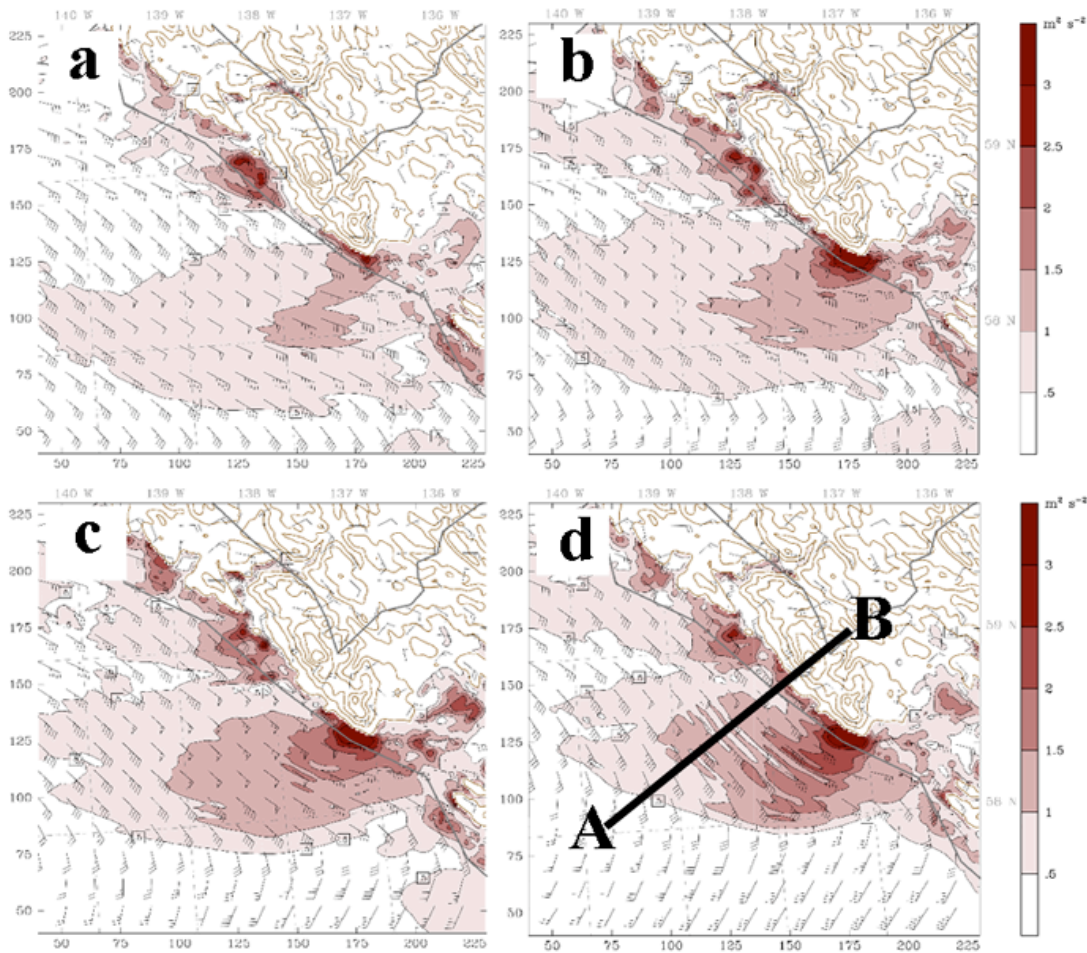


Figure 5. Winds barsbs (full barb = 5 m s^{-1}) and MYJ TKE (colored every $0.5 \text{ m}^2 \text{ s}^{-2}$) at 500 m ASL for the 1.44-km WRF-ARW at (a) 2300 UTC 12 October 2004, (b) 0000 UTC 13 October 2004, (c) 0100 UTC, and (d) 0200 UTC.

c. Model simulation of IOP7

The 1.44 km WRF-ARW reproduced the gap outflow southwest of the Fairweathers along with south-southeasterly flow of $\sim 15 \text{ m s}^{-1}$ farther offshore to the southwest (Fig. 5a). The maximum winds of the coastal jet were $\sim 26 \text{ m s}^{-1}$ at 500m MSL southwest of the Fairweathers approximately 50 km offshore (Figs. 5a,b), which was about 2 m s^{-1} less than the observations. The MYJ scheme produced the largest values of TKE in the region of the gap outflow, which rotated anticyclonically out of the coastal gap as it was modified by surface fluxes. As the weak trough moved into the region of the gap outflow (Figs. 5c,d), the coastal jet narrowed, but the maximum simulated TKE at 500 m MSL remained $\sim 3 \text{ m}^2 \text{ s}^{-2}$.

Model cross-sections of terrain-parallel wind speed (m s^{-1}), TKE ($\text{m}^2 \text{ s}^{-2}$), and potential temperature across A-B (in Fig. 5d) shows that the

jet maxima was located near $\sim 500 \text{ m ASL}$ and decayed rapidly above 1000 m ASL , with the coldest temperatures located $\sim 50 \text{ km}$ offshore (Figs. 6a,b). A layer of pronounced static stability capped the cold gap outflow (Fig. 6b). Initially, the maximum simulated TKE ($1\text{-}2 \text{ m}^2 \text{ s}^{-2}$) was located at the surface beneath the coastal jet with another maxima located in the region of reduced static stability at the coast (Fig. 6a-d). As the ambient low-level winds rotated to become more southwesterly, the region of enhanced TKE deepened due to increased shear-generated TKE at the top of the gap outflow (Fig. 6c-d).

4. Summary and Conclusions

The hybrid barrier jet case presented here shows the mean and turbulent structure of a low-level jet with maximum speeds $\sim 26 \text{ m s}^{-1}$ produced by a landfalling cyclone off of the southeastern coast of Alaska. Early in the event, the largest values of TKE were located near the surface, where cold gap

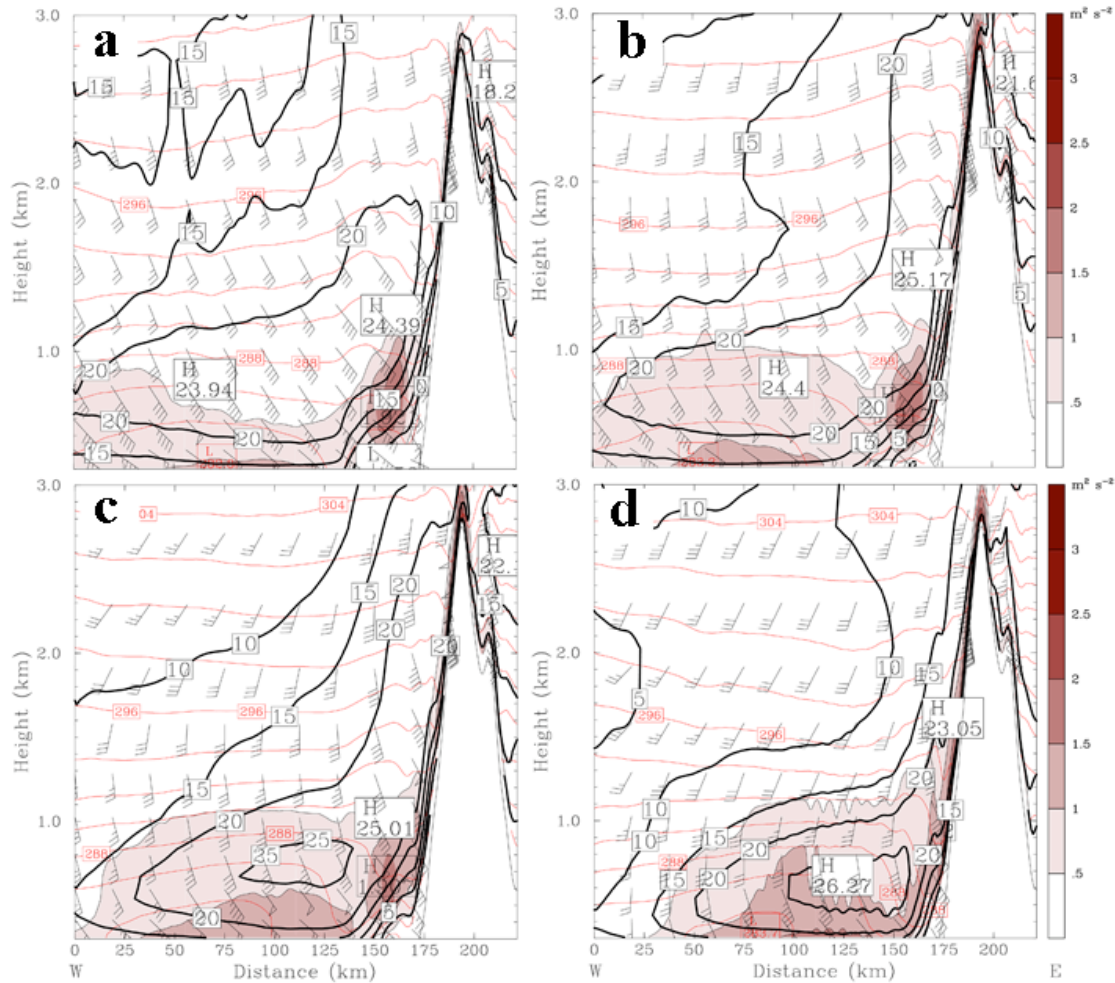


Figure 6. Vertical cross-sections taken across A-B (Fig. 5) of winds bars (full barb = 5 m s^{-1}), wind speed (black contours), potential temperature (red contours), and MYJ TKE (colored every $0.5 \text{ m}^2 \text{ s}^{-2}$) at 250 m ASL for the 1.44-km WRF-ARW at (a) 2300 UTC 12 October 2004, (b) 0000 UTC 13 October 2004, (c) 0100 UTC, and (d) 0200 UTC.

outflow over warmer SSTs resulted in buoyancy produced TKE. Later in the event, as the landfalling cyclone neared the SARJET study region, the ambient winds became oriented more southerly. This acted to increase the wind shear above the gap outflow, resulting in enhanced shear-generated TKE near in the upper portion of the jet region.

The modest agreement between the model and observations suggest a reasonable degree of skill in simulating the location and magnitude of the coastal jet and associated TKE. However, the model still was unable to capture the overall magnitude and variability of the TKE with 1.44 km resolution. Increasing the resolution from 13 to 4.33 to 1.44 km resulted in an increase of spatial and temporal variability of the TKE, but similar overall magnitudes (not shown). Also, there was only a small improvement of the barrier jet structure in the higher resolution nests, suggesting

that the proposed RR grid set up has some skill in simulating coastal jets in Alaska.

We believe the SARJET dataset is unique and may be especially valuable as a validation dataset for NWP models. Diagnosis of the WRF model errors over the complex orography of Alaska is a necessary step needed in order to further the development of the WRF-based RR. These preliminary results will be a useful benchmark for further testing of next-generation PBL schemes that will be performed in the near future. One promising aspect of these next-generation PBL schemes involve new vertical diffusion and turbulent mixing parameterizations designed for better performance in stable boundary layer conditions, which should help in the prediction of hybrid jet events off the coast of Alaska.

References

- Benjamin, S.G., D. Devenyi, S.S. Weygandt, K.J. Brundage, J.M. Brown, G.A. Grell, D. Kim, B.E. Schwartz, T.G. Smirnova, T.L. Smith, G.S. Manikin, 2004: An hourly assimilation/forecast cycle: The RUC. *Mon. Wea. Rev.*, **132**, 495-518.
- _____, D. Devenyi, T. Smirnova, S. Weygandt, J.M. Brown, S. Peckham, K. Brundage, T.L. Smith, G. Grell, and T. Schlatter, 2006: From the 13-km RUC to the Rapid Refresh. 12th Conf. on Aviation, Range, and Aerospace Meteorology, (ARAM), Atlanta, GA, Amer. Meteor. Soc. CD-ROM, 9.1
- Bond, N. A. and B. A. Walter, 2002: Research aircraft observations of the mean and turbulent structure of a low-level jet accompanying a strong storm. *J. Appl. Meteor.*, **41**, 1210-1224.
- Grell, G. A. and D. Devenyi, 2002: A generalized approach to parameterizing convection combining ensemble and assimilation techniques. *Geophys. Res. Lett.*, **29(14)**, Article 1693.
- Janjic, Z. I., 2002: Nonsingular implementation of the Mellor-Yamada level 2.5 scheme in the NCEP Meso model, *NCEP Office Note*, **No. 437**, 61 pp.
- Karacostas, T. S. and J. D. Marwitz, 1980: Turbulent kinetic energy budgets over mountainous terrain. *J. Atmos. Sci.*, **19**, 163-174.
- Loescher, K. A., G. S. Young, B. A. Colle, and N. S. Winstead, 2006: Climatology of barrier jets along the Alaskan Coast. Part I: Spatial and temporal distributions. *Mon. Wea. Rev.* **134**, 437-453.
- Macklin, S. A., N. A. Bond, and J. P. Walker, 1990: Structure of a low-level jet over lower Cook Inlet, Alaska. *Mon. Wea. Rev.*, **118**, 2568-2578.
- Mlawer, E. J., S. J. Taubman, P. D. Brown, M. J. Iacono and S. A. Clough, 1997: Radiative transfer for inhomogeneous atmosphere: RRTM, a validated correlated-k model for the longwave. *J. Geophys. Res.*, **102**, (D14), 16663-16682.
- Olson, J. B., B. A. Colle, N. A. Bond, and Nathaniel Winstead, 2007: A comparison of two coastal barrier jet events along the southeast Alaskan coast during the SARJET field experiment. *Mon. Wea. Rev.*, **135**, 3642-3663.
- _____, and Brian A. Colle, 2008: Three-dimensional idealized simulations of barrier jets along the southeastern coast of Alaska. *Mon. Wea. Rev.*, (accepted - In press).
- Overland, J. E. and N. A. Bond, 1995: Observations and scale analysis of coastal jets. *Mon. Wea. Rev.*, **42**, 271-282.
- _____, and N. A. Bond, 1993: The influence of coastal orography: The Yakutat storm. *Mon. Wea. Rev.*, **121**, 1388-1397.
- Skamarock, W. C., J. B. Klemp, J. Dudhia, D. O. Gill, D. M. Barker, W. Wang and J. G. Powers, 2005: A description of the advanced research WRF version 2. *NCAR Technical Note*.
- Thompson, G., R. M. Rasmussen, and K. Manning, 2004: Explicit forecasts of winter precipitation using an improved bulk microphysical scheme. Part I: Description and sensitivity analysis. *Mon. Wea. Rev.*, **132**, 519-542.